

USGS/NEHRP External Research Earthquake Hazards Program
Final Technical Report

Award Number: G14AP00074

Project Title: “Determining a 3D Seismic Velocity Model Offshore Southern California Using Ambient Noise”

Principal Investigator: Victor Tsai

PI affiliation:

Seismological Laboratory, MC 252-21

California Institute of Technology

Pasadena, CA 91125

Phone: (626) 395-6993

Fax: (526) 564-0715

Email: tsai@caltech.edu

Term covered by award: July 1, 2014 to December 31, 2015

Abstract

A new velocity model offshore southern California is presented that images plate boundary deformation including both thickening and thinning of the crustal and mantle lithosphere at the westernmost edge of the North American continent. The ALBACORE ocean bottom seismometer array together with 65 stations of the onshore Southern California Seismic Network are used to measure ambient noise correlation functions and Rayleigh-wave dispersion curves which are inverted for 3D shear-wave velocities. The resulting velocity model defines the transition from continental lithosphere to oceanic, illuminating the complex history and deformation in the region. A transition to the present-day strike-slip regime between the Pacific and North American Plates resulted in broad deformation and capture of the now >200-km-wide continental shelf. Our velocity model suggests the persistence of uppermost mantle volcanic processes associated with East Pacific Rise spreading adjacent to the Patton Escarpment, which marks the former subduction of Farallon Plate underneath North America. The most prominent of these seismic structures is a low-velocity anomaly underlying San Juan Seamount, suggesting ponding of magma at the base of the crust, resulting in thickening and ongoing adjustment of the lithosphere due to the localized loading. The velocity model also provides a robust framework for future earthquake location determinations and ground shaking simulations for risk estimates.

REPORT

1. Introduction

We report here on a new 3D crustal and uppermost mantle shear-wave velocity model obtained for offshore southern California. This work has the goal of defining the transition in three dimensions from continental lithospheric structure in the near shore region to oceanic structure west of the continental borderland, and contributing toward a new map of offshore southern California crustal structure for the seismological community. The velocity results are being added to the latest version of the SCEC 3D Seismic Velocity Model to provide new constraints in calculations of earthquake relocations and rupture styles, and in particular the degree to which offshore faults produce dip-slip rupture.

The tectonically active region of southern California and the Pacific-North American Plate boundary extends far west of the coastline, but seismic velocity models of the lithosphere and upper mantle in this offshore region are not well developed (from the Continental Borderland to west of the Patton Escarpment, Fig. 1), especially at subcrustal depths. This 200 km-wide offshore region represents the transition from continental lithosphere to oceanic, but is much wider than typical continental shelves and has experienced a significant amount of previous and ongoing deformation as a result of its complex history.

An array of 34 ocean bottom seismometers (OBSs) was deployed in 2010 to better understand the Pacific-North American Plate boundary deformational history and to image the region's deeper lithospheric structure. This array was part of the ALBACORE (Asthenospheric and Lithospheric Broadband Architecture from the California Offshore Region Experiment) project [Kohler et al., 2010, 2011]. The OBSs were purposely deployed far west of the coastline and the Patton Escarpment to fully capture the seismic structure transition between continental and oceanic tectonic environments.

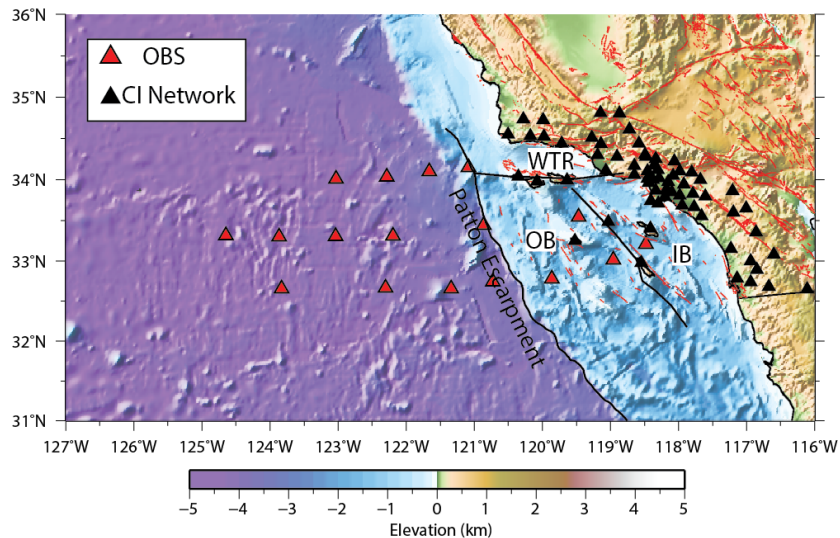


Figure 1: Map of the southern California offshore region. Triangles indicate broadband seismometers used in the study. The original ALBACORE dataset included more stations than indicated (and was roughly on a regular grid), but some stations were not recovered or indicated technical problems. OB: Outer Borderland, IB: Inner Borderland, WTR: Western Transverse Ranges.

In addition to understanding the tectonic history of the offshore region, there is also a need for accurate seismic velocity models due to its proximity to the San Andreas Fault system. The Southern California Earthquake Center (SCEC) has compiled Community Velocity Models (CVMs), with the purpose of providing a reliable base for ground motion simulations, earthquake location studies and deeper tomography. The models are well developed on-land and in the populated regions of Los Angeles, but they either end abruptly just off the coastline or they consist of an overly smooth 1D velocity profile in the offshore region.

This study uses ambient noise tomography to develop a full 3D velocity model of the region. Based on the array aperture and station spacing, we image the crust and uppermost mantle, from the oceanic lithosphere far west of the Patton Escarpment through the Inner and Outer Borderland and through continental southern California. Ocean environments tend to be noisy due to interactions between the solid earth and the water column, but ambient noise signals are recoverable at shorter periods (i.e., 5-10 s) compared to earthquake surface waves.

2. Data and Methods

Approximately one year of continuous data are used to measure ambient noise cross correlations, using data from 17 broadband ALBACORE OBS stations and 65 on-land SCSN stations (Fig. 1). Several of the OBS stations were either not recovered or contained incomplete data. Of the 34 OBSs deployed, 24 of those were broadband and 17 of those were recovered with useful data [Kohler et al., 2011]. All OBS stations used provided three components of seismic data, as well as a differential water pressure gauge (DPG) channel. In this study, only vertical component data are used for the Rayleigh wave observations. The DPG and horizontal components are used only to improve the vertical-component signals, as described below. Here we describe our signal preprocessing and dispersion curve measurement approach, the linear inversion for slowness at each period, and finally 1D depth inversions beneath each gridpoint to construct the full 3D tomographic model.

2.1 Signal Preprocessing and Cross Correlation

Underwater environments are generally very noisy due to the action of interfering swells at the surface and ocean currents at depth, and such data usually warrant additional preprocessing for ambient noise studies. While the action of water waves and subsequent pressure perturbations on the seafloor is understood to be the dominant source of ambient noise energy in the primary microseism band [Longuet-Higgins, 1950; Gimbert and Tsai, 2015], these sources are relatively well distributed in space and time across the Earth's oceans. The effect of these forces acting directly on a single OBS, however, creates an incoherent (inelastic) signal detrimental to recovering noise correlations. Fortunately, these forces from the water column are also measured by the co-located ALBACORE DPGs, so a transfer function between the two components can be used to remove the unwanted signals. Similarly, ocean currents moving past the OBS tilt the seismometer, causing low-frequency noise on the vertical channels that is incoherent with other seismometers in the array. Determining a transfer function with the horizontal components can similarly be used to remove undesired tilt signals [Webb and Crawford, 1999].

We follow the procedure of Webb and Crawford [1999] and Crawford and Webb [2000] to perform tilt corrections and DPG corrections. For a given non-vertical component (either horizontal or the DPG), a transfer function to the vertical component is determined from a 12-hour period of time known to be quiet and free of earthquakes. This transfer function describes the frequencies and associated phases at which signals are coherent, and can be used to predict the

signal that a given pressure signal or tilt event will contribute to the vertical component OBS channel (Fig. 2). The coherencies vary strongly with location and water depth, so we taper the transfer function to zero outside the period range of 5 to 15 s where the signals are most coherent. We apply all corrections in sequential steps. We first determine and apply a transfer function from one horizontal component to all other components before proceeding. Next, transfer functions from the second horizontal component are applied to both the pressure gauge and vertical component, and finally we apply the transfer function from pressure gauge to vertical. This sequential processing (i.e. also correcting one horizontal based on the other) ensures that any effect of the water column which affects both components coherently will not be mistakenly corrected twice. We also note that the transfer function is independent of units, so we do not apply the vertical instrument response until after the entire process is complete.

The effects of the wave loading and tilt corrections are often dramatic and potentially useful for event detection (Fig. 2). In contrast, we find that for the 5-9 s period range of noise cross correlations, the application of the corrections reduces the strength of the fundamental surface mode observation relative to the first overtone. It is likely that at these shorter periods our fundamental mode measurements are so sensitive to the water layer that removing signals coherent with the DPG and tilt also removes much of the useful signal. The first overtone, however, is sensitive to deeper structure and is relatively easier to measure with the correction. Thus, we consider both the uncorrected and corrected sets of noise correlations when measuring dispersion curves (Fig. 3), using whichever set shows a stronger signal at a given period.

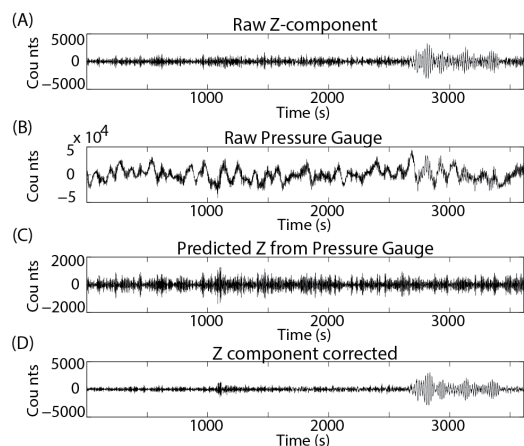


Figure 2: Steps for processing tilt and DPG corrections. An hour of uncorrected vertical component data is presented in (A). The pressure gauge component (B) is used to predict an effect on the vertical component (C) which is subtracted from the raw vertical (A) to produce a cleaned time series (D).

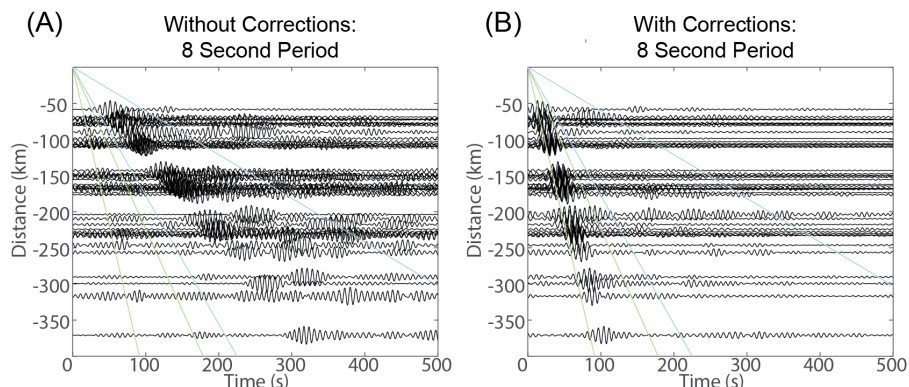


Figure 3: Record section of station pairs in the deep ocean. (A) uses raw data, (B) uses data corrected for tilt and pressure loading. We observe a very significant difference in our ability to observe the fundamental mode and first overtone, with expected ranges of velocities for both modes windowed in blue and green, respectively.

Before performing the ambient noise cross correlations, we also apply standard time-domain normalization and spectral whitening as described by Bensen et al. [2007]. These techniques help suppress the effects of earthquakes and other non-stationary sources of energy which may bias the noise correlation function (NCF). We take the symmetric component of the NCF by summing the data from positive and negative correlation time lags. We stack the entire year of data to help ensure that we have averaged out any azimuthal bias by seasonal weather patterns, even though we find that the NCFs are generally stable with 3-5 months of stacking. Measuring dispersion from the NCFs proved challenging, however, as the extremely varied tectonic nature of the region and varying water depths meant that often the arrival of a given mode could not cleanly be identified. Velocity changes created spurious reflections and scatterers in the NCFs especially in the transition region between the Borderland and coastline. Approximately half the dispersion curves were manually picked prior to application of an automated frequency-time analysis script to make a measurement. All dispersion curves were then manually reviewed. In addition to manual revisions, the signal-to-noise ratio, defined by the peak group amplitude divided by the root mean square of signals outside the expected arrival window, was measured. Band-passed measurements with $SNR < 3$ were rejected and the SNR was again subsequently used to weight pairs in the inversion. Finally, station pairs with distances less than 2 times the expected wavelength were rejected. On average approximately 1,250 raypaths were retained for a specific period based on these restrictions, out of the 3,321 total raypaths available.

Figs. 4a-c show samples of resulting dispersion measurements, grouped by pairs within distinct geologic regions. The station pairs in deeper water (Fig. 4a) are in approximately constant 4-km water depth, and are located on the relatively homogeneous abyssal plain; thus they are clean enough to distinguish the first overtone. This is particularly useful since the fundamental mode in the period range 5-10 s is dominated by the water layer (with phase velocities close to 1 km/s), while the higher modes have sensitivity primarily to crustal structure. Also, there is a gap in measurements around 10 s (Fig. 4a), which represents a transition from sensitivity predominantly to the water layer, to sensitivity to the uppermost crust. Our bandpass filters are Gaussian functions with finite width; thus, at a period of around 10 s, signals are dominated by both sensitivities' velocity and period. Figs. 4b and 4c represent raypaths in the Borderland and on-land, and show significantly more scatter due to tectonic heterogeneity.

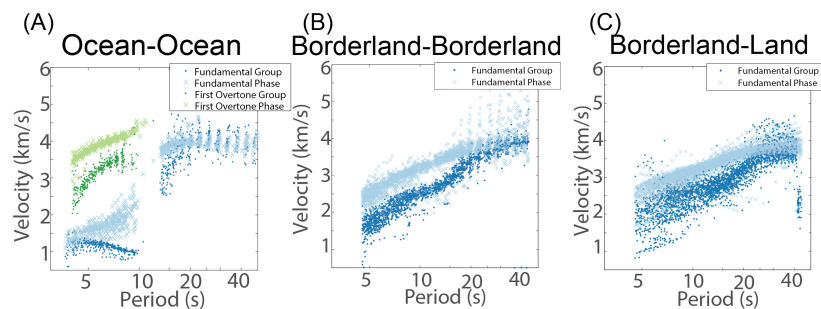


Figure 4: Sample dispersion curves grouped by dominant structural features. Raypaths not included in these figures span multiple geologic domains, such as from the deep ocean all the way onto land, and such raypaths show more variability than those presented here.

2.2 Inversion for 2D Maps at Each Period

The first step towards constructing a 3D shear-wave velocity model consisted of inverting the raypaths at 20 different periods for a 2D grid of phase and group velocity measurements, following Barmin et al. [2001] and Ma et al. [2014]. Group and phase measurements are determined at each period for both fundamental and first overtone data (e.g., Fig. 5). Velocities are described by a deviation in slowness from the average, providing a linearized inverse problem:

$$\Delta t_i = \int \frac{m_i}{c_o} ds, \leftrightarrow d = Gm$$

where $m_i = (c_0 - c)/c$ and $m = (G'WG + \beta L1'L1 + \alpha F'F)^{-1}GWd$. F describes a small amount of Gaussian smoothing applied to each ray such that it sufficiently approximates the true finite-frequency kernel [Barmin et al., 2001]. $L1$ describes a Tikhonov regularization [Loris et al., 2007], which reduces the 1st derivative across the inverted grid and stabilizes gridpoints which are outside our region of densest rays. W is a diagonal matrix of SNR used to weight better station pairs; specifically, the diagonal elements are the normalized log of $1/\text{SNR}$ to prevent overweighting. The amount of regularization is manually tuned to provide images which are smooth on the length scale of our station spacing, but with as little smoothing as possible so that the dynamic range of velocities is optimally maximized. While the conversion to slowness and the formulation of the inverse problem are linear, regularization and smoothing do not have a linear effect on the recovered velocities; however, checkerboard tests indicate this effect is minimal for our range of velocities.

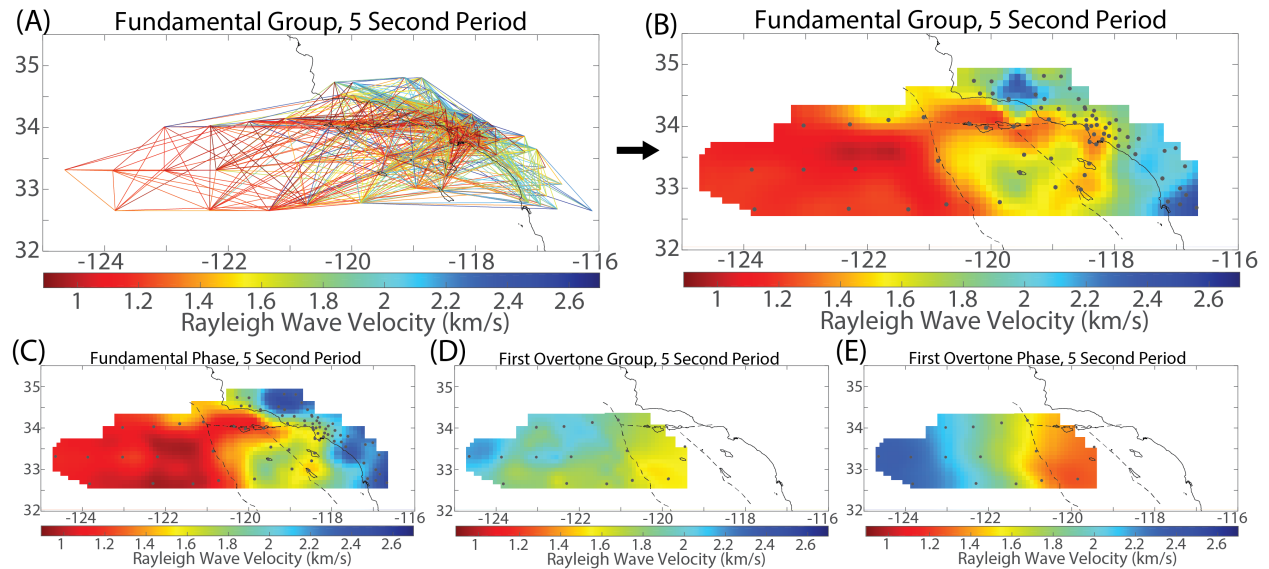


Figure 5: Examples of 2D grid inversions for a given period. Input rays shown in (A) are inverted on a regular grid, (B). The same procedure is also applied to raypath measurements of (C) fundamental phase, (D) first overtone group and (E) first overtone phase. The grid used for first overtone measurements is smaller to respect the region for which measurements were made. The same procedure is applied for 20 logarithmically spaced periods from 5s – 50s.

2.3 Inversion for Velocity with Depth

With velocities represented on a set of 2D grids, the next step towards constructing the shear-wave velocity model is to invert the dispersion curves at each grid point for 1D structure. We use a modal summation technique to compute synthetic dispersion curves and compare to data (using the software package: Computer Programs in Seismology, [Herrmann, 2013]). The inversion is allowed to iterate for each grid point, improving each 1D profile to minimize the misfit between the dispersion curve data and the synthetic dispersion curves, until the profiles converge. We use a range of 41 input starting models, all of which are linear ramps of increasing velocity or otherwise constant in velocity, linearly stepping between end member expectations of velocities between 2 km/s and 5 km/s, and whose only constraint is a water layer of fixed thickness appropriate for each grid point. We average the results from these starting models, though we find that the resulting velocity model is fairly robust and independent of starting model. We purposely use only simple starting models, as the deeper geologic structure of the region is still relatively unknown and we did not want to incorrectly bias the final model. The final model predicts dispersion data with an average misfit of 0.18 m/s, which is approximately twice as accurate as the synthetic, simple model produced from PREM and a southern California average described in supplementary material S1.

Fig. 6 shows the sensitivity kernels for our average 1D profile underneath a 4 km-thick water layer, and shows that the first overtone is considerably more sensitive to shallow crustal structure in this environment. The kernels are calculated by perturbing each layer sequentially by a 1% increase in shear-wave speed. The water layer has a shear-wave speed of zero, so the kernels' low sensitivity in the water layer is a result of no perturbation in that layer; the extremely low fundamental group and phase measurements in the short-period range is further evidence of the water sensitivity (pure water should have a phase velocity around 1.4 km/s). Both the sensitivity kernels and the resolution matrix suggest we can trust results to a depth of about 70 km, though we should expect lower resolution at the larger depths.

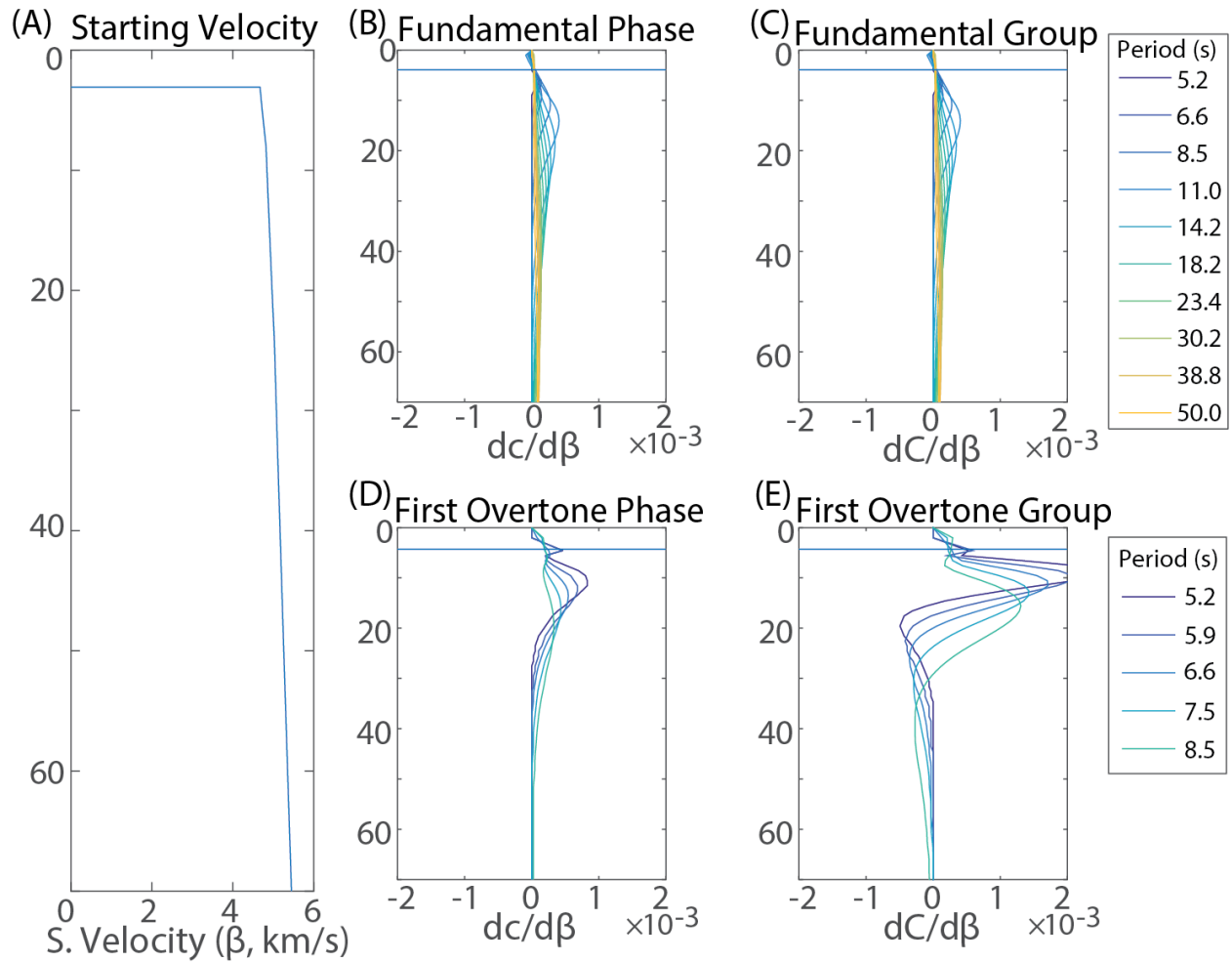


Figure 6: Depth sensitivity kernels using a 4 km thick water layer. (A) shows the starting model used, with a 4 km water depth being the predominant feature. (B) and (C) show group and phase sensitivities for the fundamental mode, while (D) and (E) show group and phase sensitivities for the first overtone.

3. Results and Discussion

Final shear-wave velocity model results are shown in Figs. 7 (plan views at different depths) and 8 (vertical cross sections). We observe that the Borderland region more closely resembles continental crust, with a distinct transition moving west to oceanic structure at the Patton Escarpment. However, the varied history of tectonic compression and extension in the Borderland leaves much variability in crustal thickness and shape.

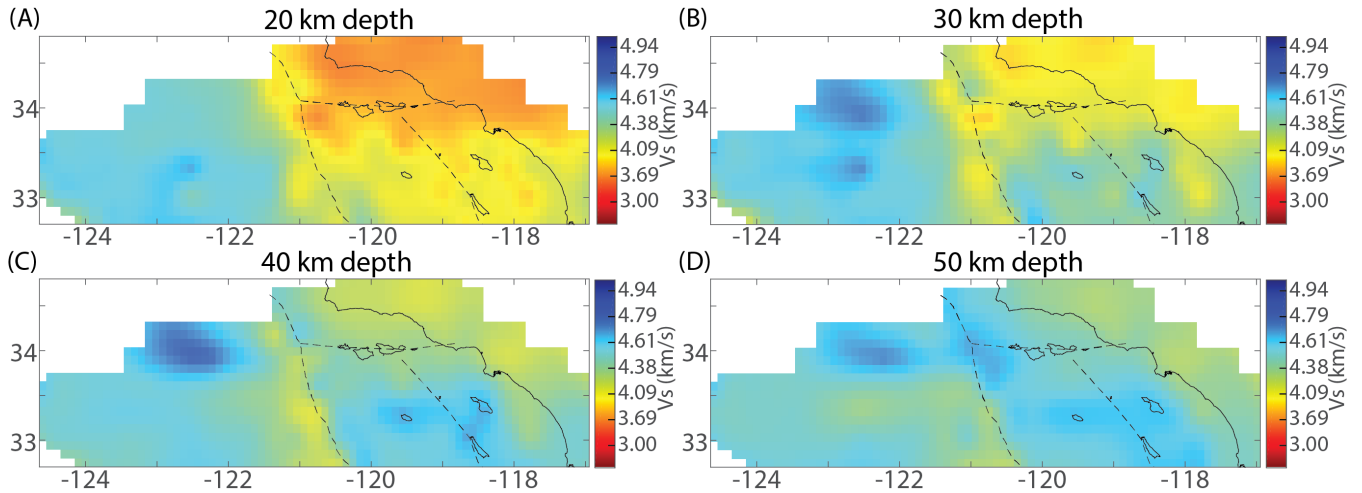


Figure 7: Plan views showing the final shear-wave velocity model at depths of 20 km (A), 30 km (B), 40 km (C) and 50 km (D).

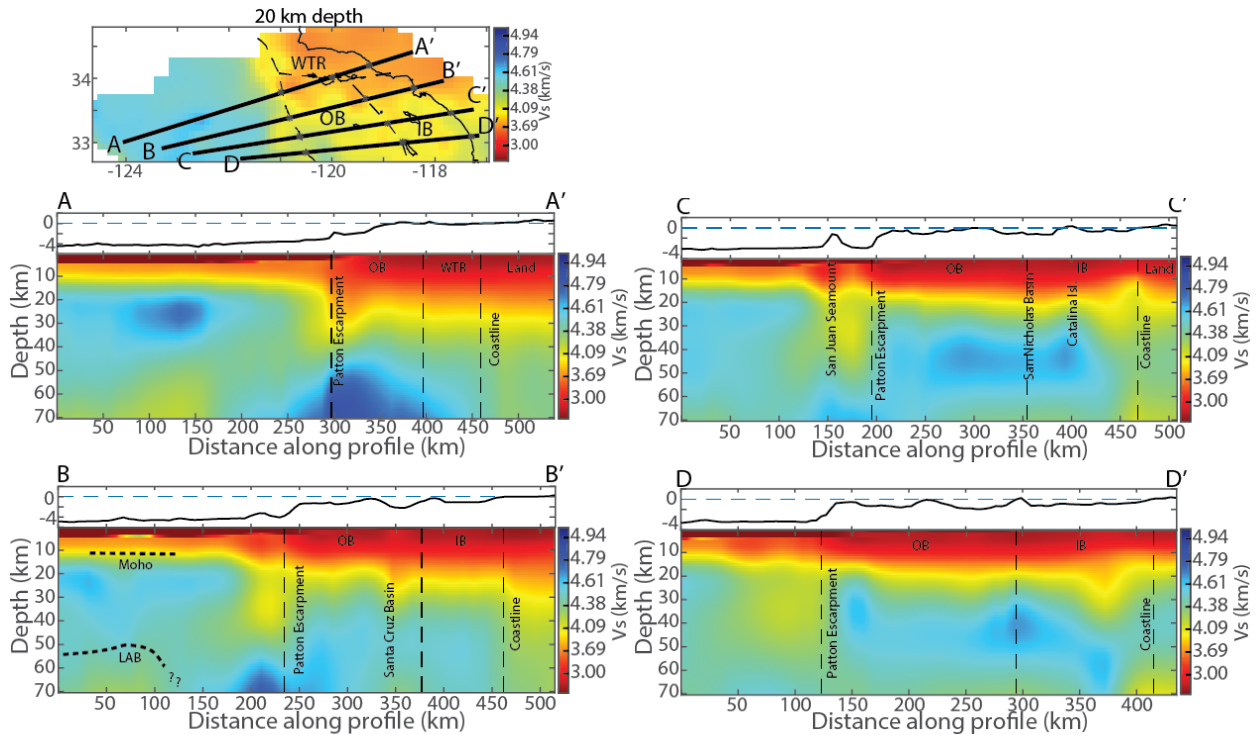


Figure 8: Profiles of the final shear-wave velocity model. Asterisks marked in map view indicate expected geologic transitions and correspond to the dashed vertical lines in cross-section.

We interpret a deeper Moho (~25 km) under the Western Transverse Ranges (Fig. 8A: profile A-A'), and crustal thinning in the Outer and Inner Borderland south of the Western Transverse Ranges (Fig. 8B-B', C-C', D-D'). This is consistent with Western Transverse Ranges capture by the Pacific Plate and subsequent rotation (i.e. [Nicholson et al., 1994]). We do not ob-

serve a crustal root as thick as is observed beneath other continental lithosphere in the region (i.e.: the on-land extent of the Transverse Ranges [Hadley and Kanamori, 1977; Raikes, 1980; Walck and Minster, 1982; Humphreys and Clayton, 1990; Kohler, 1999]), suggesting at least some deeper lithosphere was sheared away in the process of rotation. We also observe a small concentration of anomalously thicker crust, approximately 30 km thick by 30 km wide, just east of the Patton Escarpment in A-A', and interpret this as the result of pinching between the westernmost endpoint of the rotating Western Transverse Ranges block and the northward-shifting Outer Borderland. We may be seeing the velocity signature of additional thickening or shearing at the edges of a block which has been rotated more than 90 degrees. The fast anomaly at depths greater than 50 km beneath the Outer Borderland in A-A' likely relates to the same processes.

Comparing the Inner and Outer Borderland, we do not observe a significant difference in velocity structure. Nicholson et al. [1994] suggest that the Outer Borderland was laterally translated, with the bulk of extension and rotation occurring in the Inner Borderland. While our model does indicate small regions of slightly thinner crust in the Inner Borderland (profile C-C'), the difference is minimal, and we suggest that deeper crust may have subsequently flowed eastward into the Inner Borderland to equilibrate the depths of these structures, analogous to observations from the Basin and Range [Parsons, 1995], where the moho is observed to be flatter than might be expected underneath the extensional regime [Klemperer et al., 1986].

The seismic velocity model is generally consistent with gravity inversions of the USGS and LARSE lines of Miller [2002] and Romanyuk et al. [2007], both of which incorporate near-surface seismic reflection data, borehole measurements, and magnetic anomalies. For example, the depth of the Moho, and the sloping increase in this depth across the coastline are evident in both models (Fig 8C, profile C-C', between horizontal distances of 400 and 450 km). We also observe a fast anomaly in the Santa Cruz Basin (Fig. 8B, profile B-B', at a horizontal distance of 350 km) with a depth of 2-10 km, which Miller [2002] interprets as an outcrop of volcanic rocks, consistent with borehole measurements from Bohannon and Geist [1998]. Unlike the gravity inversions however, we observe a lower-velocity structure beneath the Santa Cruz Basin to a depth of 50 km, which we interpret as isostatic compensation for the denser shallow material above.

The existence of a remnant, thin, Farallon slab underplating either part of or the entire region is a subject of much debate [e.g., Bohannon and Parsons, 1995; Fuis, 1998; ten Brink et al., 2000; Nazareth and Clayton, 2003; Romanyuk et al., 2007]. We do not observe evidence for such a layer. A remnant slab would be observable as a thin, high-velocity layer at somewhere between 10-20 km depths. Even though our method lacks sharp resolution at this depth range, an underplated slab with a strong velocity contrast should still be evident, even if smoothed or blurred in our results. We also generally observe highly variable Moho depths under the Borderland. If any underplated slab exists, it must have been subject to the same deformation, thinning and isostatic compensation as the rest of the adjacent lithosphere, making it potentially difficult to image by this or any other technique.

The western side of our study region is characterized by fossil spreading center segments, volcanism and fracture zones associated with the East Pacific Rise (EPR), which stopped spreading approximately 18-20 Ma [Atwater, 1989; Atwater and Stock, 1998; Lonsdale, 1991]. Three seamounts that resulted from EPR volcanic activity lie within the study region: the San Juan Seamount on the Pacific Plate, the Rodriguez Seamount lying on the continental slope, and the Northeast Bank Seamount located within the Continental Borderland. Our velocity model suggests the persistence of uppermost mantle volcanic processes associated with EPR spreading and fracture zones. The most prominent of these seismic structures is a low-velocity anomaly under-

lying San Juan Seamount that can be traced throughout each cross section (e.g., Fig. 8C between horizontal distances 150 and 180 km). The low-velocity anomaly is about 30 km wide and has a depth extent of 50 km, well within good resolution limits. A low-velocity seismic structure is observed below the Rodriguez Seamount (Fig. 8A) but the depth and lateral extent are complicated by the seamount's location at the endpoint of the rotating Transverse Ranges tectonic block [Nicholson et al., 1994]. No clear low-velocity anomaly is observed below Northeast Bank. This may be due to its location within the continental Borderland which has undergone extension and rotation, resulting in decoupling with underlying mantle flow processes. The San Juan Seamount is part of a chain of nine seamounts with NE-SW orientation off the coast of central and southern California. The seamounts were once islands that were the product of small-volume volcanic eruptions due to decompression melting of suboceanic mantle melts rising along zones of weakness in the oceanic crust [Paduan et al., 2009; Davis et al., 2010]. On the San Juan Seamount there is geochemical evidence for eruptions as recent as 2.8 Ma [Paduan et al., 2009; Davis et al., 2010]; thus our images may be showing thermal or chemical signatures of mantle upwelling of this age. The low-velocity anomaly is located laterally where mantle lithosphere is expected to thin between the Outer Borderland and Pacific oceanic plate to the west. Our images suggest a mantle lithosphere thickness, inferred from the seismic wave speeds, of at least 70 km below the region adjacent to and west of the Patton Escarpment as well as below the Outer Borderland, and 60 km below the Pacific Plate. The presence of small-scale mantle flow may be producing heterogeneous crustal and mantle lithospheric thicknesses below both oceanic and continental tectonic regimes.

4. Incorporation into the SCEC Community Velocity Model (CVM)

The new velocity model presented here provides the first complete view of the deeper seismic structure well offshore southern California, and provides a basis for future inversions and modeling with joint datasets. It is in the process of being added to the latest version of the SCEC 3D Seismic Velocity Model to provide new constraints in calculations of earthquake relocations and ground shaking simulations for assessing risk associated with offshore faults

SCEC is currently undergoing a major overhaul of its CVM framework, including the UCVM software collection tools designed to request velocity model parameters for any given 3D location. SCEC Executive Science Director for Special Projects Christine Goulet is directing SCEC software engineers in this long-term effort. Since it will take many months before the final updated SCEC CVM infrastructure is in place, we are working with Dr. Goulet on both short-term and long-term solutions to integrating our model with existing southern California models. The short-term solution consists of making our model available in stand-alone format such that it can be downloaded on its own, analogous to other stand-alone velocity models. To that end, the model will be made publicly available as a 3D grid of points with V_s (as determined by the inversions), V_p (using a rule-based function for V_p/V_s ratio), and density (also rule-based depending on seismic velocity). To complement this effort, we are working with SCEC to create a model-specific SCECpedia page (e.g., https://scec.usc.edu/sceclopedia/UCVM#SCEC_CVM-S4) that describes the model and contains the link to it. The long-term solution is to include it in the growing collection of SCEC velocity models such that the UCVM software tool can stitch it together with other existing models into a physically realistic, numerically stable, consolidated model that is customized to each end-user's scientific goals.

5. References

- Atwater, T. (1989), Plate tectonic history of the northeast Pacific and western North America, *East. Pacific Ocean Hawaii Boulder, Color. Geol. Soc. Am. Geol. North Am. v. N*, 21–72.
- Atwater, T., and J. Stock (1998), Pacific-North America Plate Tectonics of the Neogene Southwestern United States: An Update, *Int. Geol. Rev.*, 40(5), 375–402, doi:10.1080/00206819809465216.
- Barmin, M. P., M. H. Ritzwoller, A. L. Levshin, (2001), A fast and reliable method for surface wave tomography, *Pure Appl. Geophys.*, 158(8), 1351–1375, doi:http://dx.doi.org/10.1007/PL00001225.
- Bensen, G. D., M. H. Ritzwoller, M. P. Barmin, a. L. Levshin, F. Lin, M. P. Moschetti, N. M. Shapiro, and Y. Yang (2007), Processing seismic ambient noise data to obtain reliable broad-band surface wave dispersion measurements, *Geophys. J. Int.*, 169(3), 1239–1260, doi:10.1111/j.1365-246X.2007.03374.x.
- Bohannon, R. G., and E. Geist (1998), Upper crustal structure and Neogene tectonic development of the California continental borderland, *Geol. Soc. Am. Bull.*, 110 (6), 779–800, doi:10.1130/0016-7606(1998)110<0779:UCSANT>2.3.CO;2.
- Bohannon, R. G., and T. Parsons (1995), Tectonic implications of post-30 Ma Pacific and North American relative plate motions, *Geol. Soc. Am. Bull.*, 107 (8), 937–959, doi:10.1130/0016-7606(1995)107<0937:TIO PMP>2.3.CO;2.
- Crawford, W. C., and S. C. Webb (2000), Identifying and Removing TiltNoise from Low Frequency LT0.1Hz Seafloor Vertical Seismic Data, *Bull. Seismol. Soc. Am.*, 90(4), 952–963.
- Davis, A. S., D. A. Clague, J. B. Paduan, B. L. Cousins, and J. Huard (2010), Origin of volcanic seamounts at the continental margin of California related to changes in plate margins, *Geochem. Geophys. Geosyst.*, 11(5), Q05006, doi:10.1029/2010gc003064.
- Fuis, G. S. (1998), West margin of North America — a synthesis of recent seismic transects, *Tectonophysics*, 288(1-4), 265–292, doi:10.1016/S0040-1951(97)00300-4.
- Gimbert, F., and V. C. Tsai (2015), Predicting short-period, wind-wave-generated seismic noise in coastal regions, *Earth Planet. Sci. Lett.*, 426, 280–292, doi:10.1016/j.epsl.2015.06.017.
- Hadley, D., and H. Kanamori (1977), Seismic structure of the Transverse Ranges, California, *Geol. Soc. Am. Bull.*, 88 (10), 1469–1478, doi:10.1130/0016-7606(1977)88<1469:SSOTTR>2.0.CO;2.
- Herrmann, R. B. (2013), Computer Programs in Seismology: An Evolving Tool for Instruction and Research, *Seismol. Res. Lett.*, 84(6), 1081–1088, doi:10.1785/0220110096.
- Humphreys, E., and R. Clayton (1990), Tomographic Image of the Southern California Mantle, *J. Geophys. Res.*, 95(B12), 19725–19746.
- Klemperer, S. L., Hauge, T. A., Hauser, E. C., Oliver, J. E., & Potter, C. J. (1986). The Moho in the northern Basin and Range province, Nevada, along the COCORP 40 N seismic-reflection transect. *Geological Society of America Bulletin*, 97(5), 603-618.
- Kohler, M. D. (1999), Lithospheric deformation beneath the San Gabriel Mountains in the southern California Transverse Ranges, *J. Geophys. Res.*, 104(B7), 15025, doi:10.1029/1999JB900141.
- Kohler, M., K. Booth, C. Sun, C. Curl, C. Finnell, P. Shute, W. B. Prine, J. Ramos, and W. Brown (2011), ALBACORE OBS Deployment Cruise Report, *R/V Melville* Cruise MV1010, 27 pp., 14-27 Aug. 2010
- Kohler, M., K. Brunner, M. Donohue, D. Weaver, T. Chi, and M. Breen (2012), ALBACORE OBS Recovery Cruise Report, *R/V New Horizons* Cruise NH1111, 35 pp., 7-16 Sept. 2011

- Longuet-Higgins, M. S. (1950), A Theory of the Origin of Microseisms, *Philos. Trans. R. Soc. London A Math. Phys. Eng. Sci.*, 243(857), 1–35, doi:10.1098/rsta.1979.0079.
- Lonsdale, P. (1991), Structural patterns of the Pacific floor offshore of Peninsular California, in: “The Gulf and Peninsular Province of the Californias,” (chapter 7), Edited by J. P. Dauphin and B. R. T. Simoneit, AAPG Memoir, 47, 87-125.
- Loris, I., Nolet, G., Daubechies, I., and Dahlen, F. A. (2007). Tomographic inversion using ℓ_1 -norm regularization of wavelet coefficients. *Geophysical Journal International*, 170(1), 359-370.
- Miller, K. (2002), Geophysical evidence for Miocene extension and mafic magmatic addition in the California Continental Borderland, *Geol. Soc. Am. Bull.*, 114(4), 497–512, doi:10.1130/0016-7606(2002)114<0497:GEFMEA>2.0.CO;2.
- Nazareth, J. J., and R. W. Clayton (2003), Crustal structure of the Borderland-Continent transition zone of southern California adjacent to Los Angeles, *J. Geophys.*, 108, B8, 2404 doi:10.1029/2001JB000223.
- Nicholson, C., C. C. Sorlien, T. Atwater, J. C. Crowell, and B. P. Luyendyk (1994), Microplate capture, rotation of the western Transverse Ranges, and initiation of the San Andreas transform as a low-angle fault system, *Geology*, 22(6), 491–495, doi:10.1130/0091-7613(1994)022<0491:MCROTW>2.3.CO;2.
- Paduan, J. B., D. A. Clague, and A. S. Davis (2009), Evidence that three seamounts off southern California were ancient islands, *Mar. Geol.*, 265(3-4), 146–156, doi:10.1016/j.margeo.2009.07.003.
- Parsons, T. (1995). The basin and range province. *Continental rifts: evolution, structure, tectonics*, 25, 277-324.
- Raikes, S. A. (1980), Regional variations in upper mantle structure beneath Southern California, *Geophys. J. R. astr. Soc.*, 63, 187-216.
- Romanyuk, T., W. D. Mooney, and S. Detweiler (2007), Two lithospheric profiles across southern California derived from gravity and seismic data, *J. Geodyn.*, 43(2), 274–307, doi:10.1016/j.jog.2006.09.011.
- ten Brink, U. S., J. Zhang, T. M. Brocher, D. A. Okaya, K. D. Klitgord, and G. S. Fuis (2000), Geophysical evidence for the evolution of the California Inner Continental Borderland as a metamorphic core complex, *J. Geophys. Res.*, 105 (1999), 5835–5857, doi:10.1029/1999JB900318
- Walck, M. C., and J. B. Minster (1982), Relative array analysis of upper mantle lateral velocity variations in Southern California, *J. Geophys. Res.*, 87, 1757-1772.
- Webb, S. C., and W. C. Crawford (1999), Long-period seafloor seismology and deformation under ocean waves, *Bull. Seismol. Soc. Am.*, 89(6), 1535–1542.

Bibliography of publications from this award:

Bowden, D. C, M. D. Kohler, V. C. Tsai, and D. S. Weeraratne, Offshore southern California lithospheric velocity structure from noise cross correlation functions, *J. Geophys. Res.*, submitted, 2016.